

Article

Feasibility of Recycling Bayer Process Red Mud for the Safety Backfill Mining of Layered Soft Bauxite under Coal Seams

Shuai Li , Rui Zhang , Ru Feng, Boyi Hu * , Guojun Wang and Haoxuan Yu 

School of Resources and Safety Engineering, Central South University, Changsha 410083, China; shuaige@csu.edu.cn (S.L.); 8210183027@csu.edu.cn (R.Z.); ru-feng@csu.edu.cn (R.F.); 8210183012@csu.edu.cn (G.W.); yuhaoxuan@csu.edu.cn (H.Y.)

* Correspondence: boicary@csu.edu.cn

Abstract: The mining of layered soft bauxite under coal seams (BCS) will cause serious underground goaf disasters and surface Bayer process red mud (BRM) pollution. In order to realize the safe and efficient mining of BCS, the feasibility of recycling BRM as a backfilling aggregate was explored. A series of tests were conducted to prevent the pollution diversion of BRM from surface storage to underground goafs, and a numerical simulation analysis of the backfilling mining process was carried out based on FLAC^{3D} to protect the overlying coal seam. The results show that: under the action of encapsulation, solidification and inhibiting precipitation from cementitious materials, the leaching concentration of harmful substances in red mud-based cemented backfill (RCB) can be reduced 70% more than fresh BRM. Mining disturbance redistributes the in-situ stress field of overlying strata; normal backfilling can not only reduce the pressure stress of pillars, but also release the tensile stress in the roof and floor from +0.4956 MPa to −0.1992 MPa, effectively preventing roof subsidence. Since the creep damage process of past backfill will absorb and dissipate lots of energy, the disturbance range caused by backfill mining is controlled within 3 m, which is only 10% of the open-stope method.

Keywords: Bayer process red mud (BRM); red mud-based cemented backfill (RCB); backfill mining technology; layered soft rocks; bauxite under coal seams (BCS)



Citation: Li, S.; Zhang, R.; Feng, R.; Hu, B.; Wang, G.; Yu, H. Feasibility of Recycling Bayer Process Red Mud for the Safety Backfill Mining of Layered Soft Bauxite under Coal Seams. *Minerals* **2021**, *11*, 722. <https://doi.org/10.3390/min11070722>

Academic Editor: Abbas Taheri

Received: 16 May 2021

Accepted: 30 June 2021

Published: 5 July 2021

Publisher's Note: MDPI stays neutral with regard to jurisdictional claims in published maps and institutional affiliations.



Copyright: © 2021 by the authors. Licensee MDPI, Basel, Switzerland. This article is an open access article distributed under the terms and conditions of the Creative Commons Attribution (CC BY) license (<https://creativecommons.org/licenses/by/4.0/>).

1. Introduction

As the world's largest producer and consumer of alumina, China's total output of alumina in 2020 was 70.353 million tons, accounting for about 52.5% of the world's total output. However, China's bauxite reserves are less than three percent of the world's total, and 98% of them are diasporic bauxite with poor quality, difficult processing and high energy consumption. Different from lateritic bauxite ores in foreign countries, bauxite ores in China are mainly an ancient weathering crust, and industrial coal seams are often produced in the overlying strata [1]. For example, nearly 2/3 of the bauxite deposits in Shanxi and Henan provinces, which account for about half of China's reserves, belong to bauxite under coal seams (BCS). In order to protect the safety of the overlying coal seam, a large number of pillars are left to support the roof, thereby causing loss to the plentiful mineral resources. Additionally, continuous high-intensity mining can also produce large mined-out area groups of accumulating roof caving, and collapse accidents extremely easily, leading to overlying roof bending deformation, damage, and the overall fall. Furthermore, it may run through the overlying coal seam and generate gas outburst disaster, surface subsidence, and collapse, causing serious damage to surface rivers, highways, and structures [2].

At present, 95% of the world's aluminum companies are using the Bayer process to treat bauxite ore to produce alumina, and the solid waste produced is called Bayer process red mud (BRM). BRM contains a large amount of free alkali, chemically bound alkali which are difficult to remove. Open-air stockpiling not only takes up a lot of land, but also easily causes serious pollution to the surface environment [3]. In consideration of

its latent hydration properties, BRM has been used for developing effective adsorbents [4], producing cements [5], building bricks [6], glasses, and special ceramics [7], as well as additives or excipients for asphalt materials, roadbed materials [8], thermal insulation materials, and other building materials. However, due to the complex process and low number of value-added products, it's a great challenge to obtain economic benefits during the comprehensive utilization process of BRM. As a consequence, the annual production of BRM in China is up to 60 million tons, while the comprehensive utilization rate is only 10% [9]. Consequently, it is particularly urgent to minimize the harm of BRM and realize its multi-channel and large-scale utilization. Further, the concentrations of chlorides and fluorides in the BRM filtrate, which may pollute the groundwater nearby, were also detected and far exceed the recommended groundwater quality standards of China [10,11].

Cemented backfill mining is a well-proportioned mixture of solid aggregates, cementing materials, and water, and is transported from the surface backfilling station to underground mining goafs in a pipeline [12]. After osmotic dehydration and consolidation hardening, cemented backfill shows excellent superiority in ground pressure management and mining safety guarantee [13]. Meanwhile, cemented backfill also provides an environment-friendly, economic, and feasible way for the large-scale disposal and utilization of bulky industrial solid wastes. The lead zinc tailings, which contain a great quantity of heavy metal ions, were used as a backfilling aggregate for underground backfill mining for more than 15 years in the Huize mine in the Yunnan province [14]. In many provinces of China, coal mines are required to reuse coal gangues and fly ash for backfill mining to prevent surface subsidence and collapse [15]. Smelting slags, which are calcined at a high temperature and rapidly cooled by water quenching, show superior cementitious activity and can be reused for backfill mining as new cements [16]. As a strong acid solid waste, phosphogypsum has been used as a backfilling aggregate for more than 10 years in the Kaiyang mine in the Guizhou province, which provides a significant demonstration for the safe disposal of BRM [17].

However, owing to the unique properties of BRM, no successful practical application has been found for red mud-based cemented backfill (RCB) using such a type of BRM. Whether BRM can be used for backfill mining, the primary challenge is to prevent the pollution diversion of BRM from surface storage to underground goafs, and avoid polluting the groundwater. The second task is to improve the early strength of RCB and ensure the mining safety of layered soft BCS. Therefore, a full understanding of its material characteristics, mixture parameters, rheological behavior, and pollution episodes is necessary before the practical application of RCB. The objective of this study is to realize the safe and efficient mining of layered soft BCS. The feasibility of recycling BRM as a backfilling aggregate was explored by a lot of tests, and a numerical simulation analysis of the backfilling mining process was carried out based on the FLAC^{3D} software.

2. Mixture Proportion Tests and Groundwater Pollution Analysis of RCB

To explore the feasibility of BRM as a backfilling aggregate, the following tests, shown in Figure 1, were carried out using the BRM of an aluminum oxide plant in Shanxi. First of all, tests on the physical properties, chemical composition, and SEM microstructure of BRM were carried out to explore its material characteristics (see Table 1). Then, a series of mixture proportion tests were carried out to obtain the optimum mass concentration and cement–sand ratio of RCB. Additionally, the rheological behavior of RCB was evaluated according to the collapse, shear rheology, and L Tube tests [18]. Finally, the effect of RCB on the environmental safety of groundwater was analyzed due to the results of bleeding, leaching toxicity, and immersion tests (see Figure 2) [19,20].

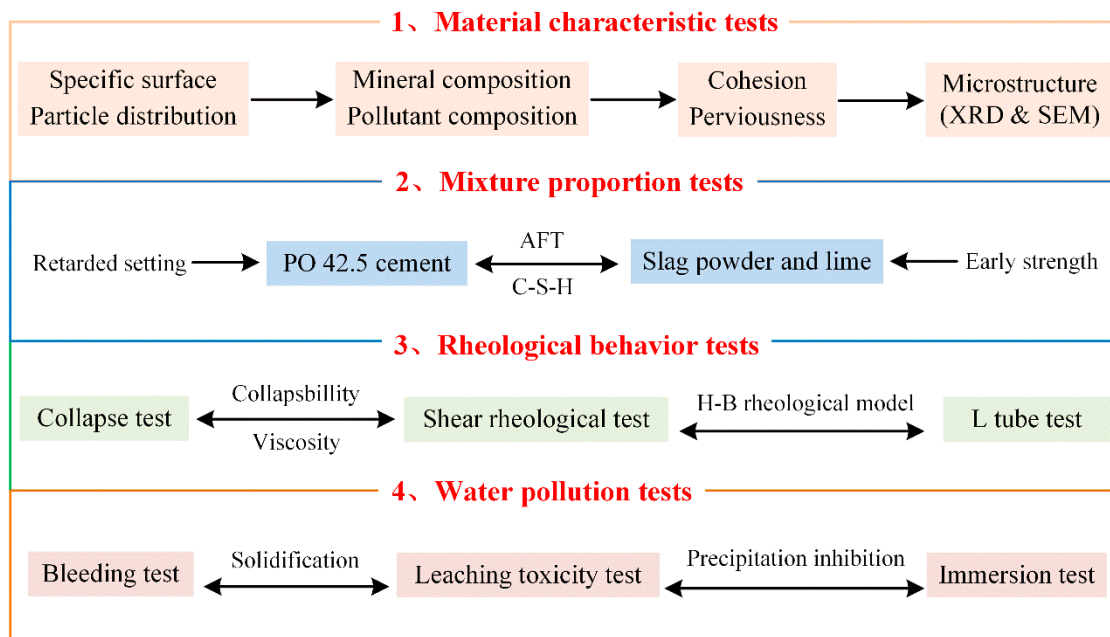


Figure 1. Laboratory test process of RCB.

Table 1. Physical properties of BRM.

Permeability Coefficient (cm/s)	Median Particle Size (µm)	Specific Surface Area (m ² /kg)	Nonuniform Coefficient	Curvature Coefficient
3.35×10^{-7}	3.248	2940	4.741	0.946

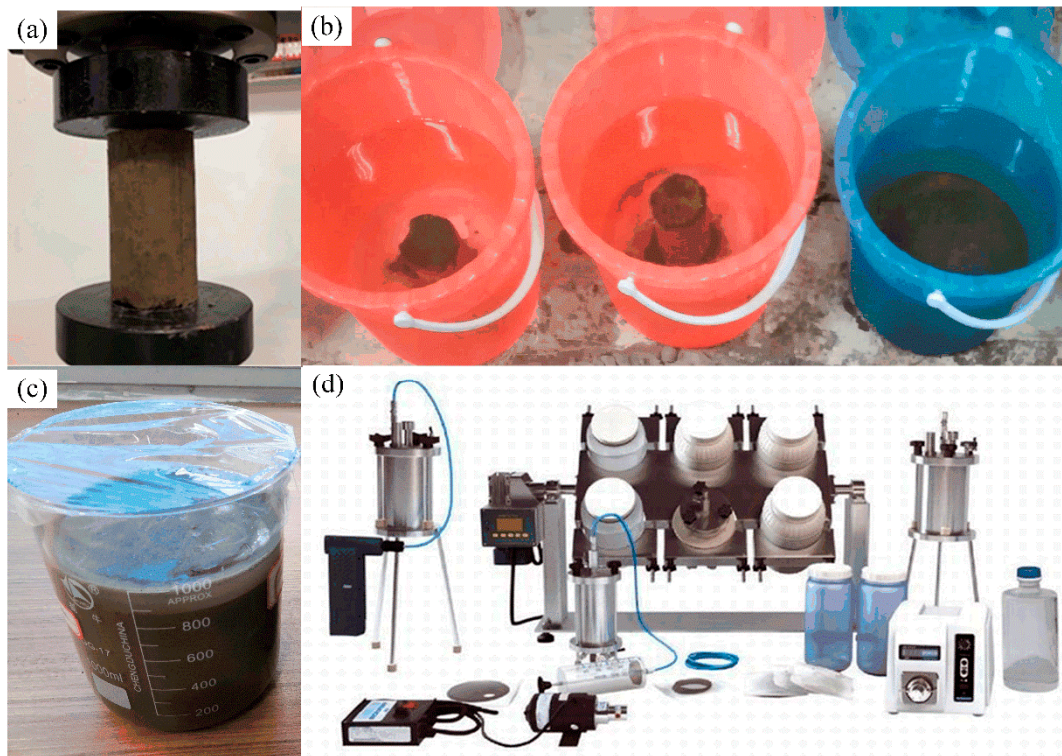


Figure 2. Contamination analysis experiments of RCB: (a) uniaxial compressive strength test; (b) immersion tests; (c) bleeding test; (d) leaching toxicity test.

The material characteristic tests represented that: the particle size of BRM is superfine, 88% of which is below 15 μm , and the median diameter is just 3.248 μm [21]. With a specific area of 2940 m^2/kg , the porosity of BRM is much larger than that of common soil. Further, the density of BRM is 2.38 t/m^3 , the plasticity index is 17.0~30.0, and the osmotic coefficient is only 3.35×10^{-5} cm/s . As a strong alkaline solid waste produced by the alumina industry, BRM contains plenty of alumina, iron oxide, titanium dioxide, sodium oxide, and calcium oxide [22]. Traditional PO 42.5 cement shows a slow solidifying rate and low early strength when mixed with BRM. By using S95 slag powder (account for 90%) as the cementitious material, and lime (account for 10%) as the activator, the compressive strength of RCB with a cement–sand ratio of 1:6 and 60% mass concentration solidified quickly within 12 h and reached a high strength of 1.1 MPa in 7 days. The rheological behavior tests indicate that, RCB shows obvious time-varying shear thinning characteristics, which is suitable for the Herschel–Bulkley rheological model [23].

The contents of several common heavy metal ions, pH values, fluoride, chloride, nitrate, nitrite, sulfate, ammonia nitrogen, chloride, and other contaminants were detected, and the results of the bleeding and immersion tests are shown in Table 2.

Table 2. Results of bleeding and immersion tests (unit: mg/L).

Indicators	Mine Groundwater	Bleeding Water	Immersing Water	Groundwater Quality Standard of China				
				I	II	III	IV	V
pH value	7.75	11.68	11.58		6.5~8.5		5.5~6.5 8.5~9.0	<5.5 >9.0
Ammonia nitrogen	0.37	0.56	0.41	≤ 0.02	≤ 0.1	≤ 0.5	≤ 1.5	> 1.5
Nitrate	0.045	2.71	1.97	≤ 2.0	≤ 5.0	≤ 20.0	≤ 30.0	> 30
Nitrite	0.029	1.20	0.12	≤ 0.01	≤ 0.10	≤ 1.00	≤ 4.80	> 4.8
Fluoride	0.16	<0.05	<0.05	≤ 1.0	≤ 1.0	≤ 1.0	≤ 2.0	> 2.0
Sulfate	5.54	204.37	12.77	≤ 50	≤ 150	≤ 250	≤ 350	> 350
Chloride	11.64	19.94	11.37	≤ 50	≤ 150	≤ 250	≤ 350	> 350
Na	154.2	276.35	158.55	≤ 100	≤ 150	≤ 200	≤ 400	> 400
Fe	0.18	0.055	0.046	≤ 0.1	≤ 0.2	≤ 0.3	≤ 2.0	> 2.0
Cu	<0.001	<0.001	<0.001	≤ 0.01	≤ 0.05	≤ 1.00	≤ 1.50	> 1.50
Zn	<0.001	<0.001	<0.001	≤ 0.05	≤ 0.5	≤ 1.00	≤ 5.00	> 5.00
As	<0.001	<0.001	<0.001	≤ 0.001	≤ 0.001	≤ 0.01	≤ 0.05	> 0.05
Cd	<0.001	<0.001	<0.001	≤ 0.0001	≤ 0.001	≤ 0.005	≤ 0.01	> 0.01
Pb	<0.001	<0.001	<0.001	≤ 0.005	≤ 0.005	≤ 0.01	≤ 0.1	> 0.1

As shown in Figure 3, after mixed with S95 slag powder, lime, and water at a certain ratio at a high speed, RCB is produced and transported via pipage through surface drilling and underground laneways to a mining goaf. As a strong alkaline solid waste, BRM contains fluoride, heavy metal ions, and other substances, and can easily pollute the surface environment by the way of open-air storage [24]. However, due to the groundwater recycling process of RCB, RCB will not transfer the surface pollution to the underground. The main reasons are as follows:

- (1) A large number of S95 slags are added and mixed with BRM, which will produce a large number of ettringite, C-S-H gel, and other hydration products and have a significant effect on the encapsulation and solidification of pollutants in BRM [25,26]. The leaching toxicity test results show that the leaching concentration of harmful substances in RCB can be reduced 70 % more than fresh BRM.
- (2) In order to improve the backfilling effect and reduce the bleeding water, RCB is generally prepared into a paste state. After entering the goaf, only a small amount of bleeding water will be discharged through the basket drain embedded in the filter wall. According to estimates, the bleeding rate is less than 5% and the bleeding flow is less than 0.1 t/h.

- (3) The bleeding water has a high pH value, and the contents of ammonia nitrogen, nitrite, and sodium belong to the grade IV groundwater standard of China. Therefore, bleeding water must be discharged uniformly through the gutterway to the central water sump. After entering the water sump, the bleeding water will be mixed with the mining gushing water, fault drainage water, and goaf water, causing a dilution effect. According to the different water inflow, the dilution ratio can reach at least 50–100 times, and the water quality after dilution belongs to the grade I groundwater standard of China.
- (4) The gushing water in the water sump will be periodically discharged to the surface sewage tank for centralized purification treatment, and recycled for backfill or underground production, realizing the total recycling and zero discharge of groundwater.

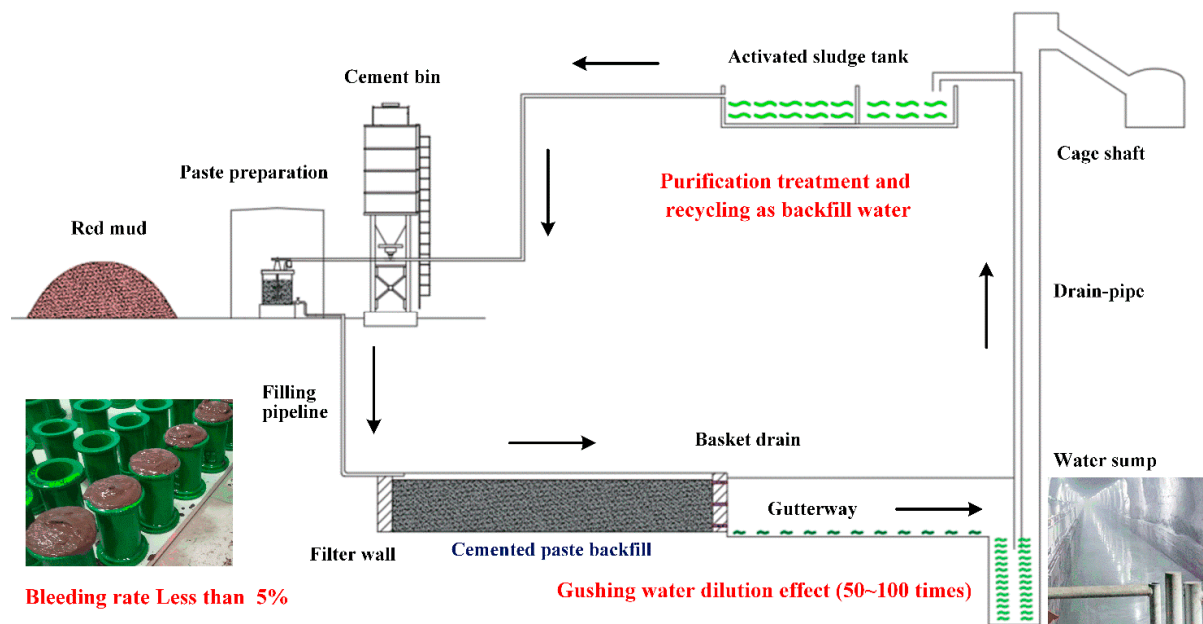


Figure 3. Groundwater recycling process of RCB.

3. Mining Safety Simulation of Layered Soft BCS

3.1. Engineering Geological Condition

As typical ancient weathering crust-type bauxite deposits, 70% of the bauxite resources in the Shanxi province belong to BCS [27]. Taking a typical bauxite mine in Shanxi as an example, the deposit occurs in the lower part of the Benxi formation of the Carboniferous middle series, which is unconformable in contact with the erosion surface of Ordovician limestone and iron clay rock at the bottom. As we can see from Figure 4, the overlying strata are composed of clay rock (C_2b^1) and mudstone (C_2b^2) of the Benxi formation, mudstone (C_3t^1) and sandstone (C_3t^2) of the Taiyuan formation, laterite (N_2) of Neogene, and loess (Q_3) of Quaternary. The ore quality is medium with an Al_2O_3 content of 65% and an alumina–silica ratio of 5.5. The bauxite orebody average thickness is 2.85 m, the average dip angle is 7° , while the overlying 13# coal seam is 6.10 m thick and 53 m away from the bauxite orebody. With a low ultimate tensile strength of 0.48 MPa and softening coefficient of 0.53, the orebody roof is soft, weak, and unstable. The in-strips drift backfilling method (IDBM) is selected as the main mining method. Due to the two-step interval process of IDBM, high-strength RCB is adopted in the first step, while low-strength RCB is adopted in the second step [28].

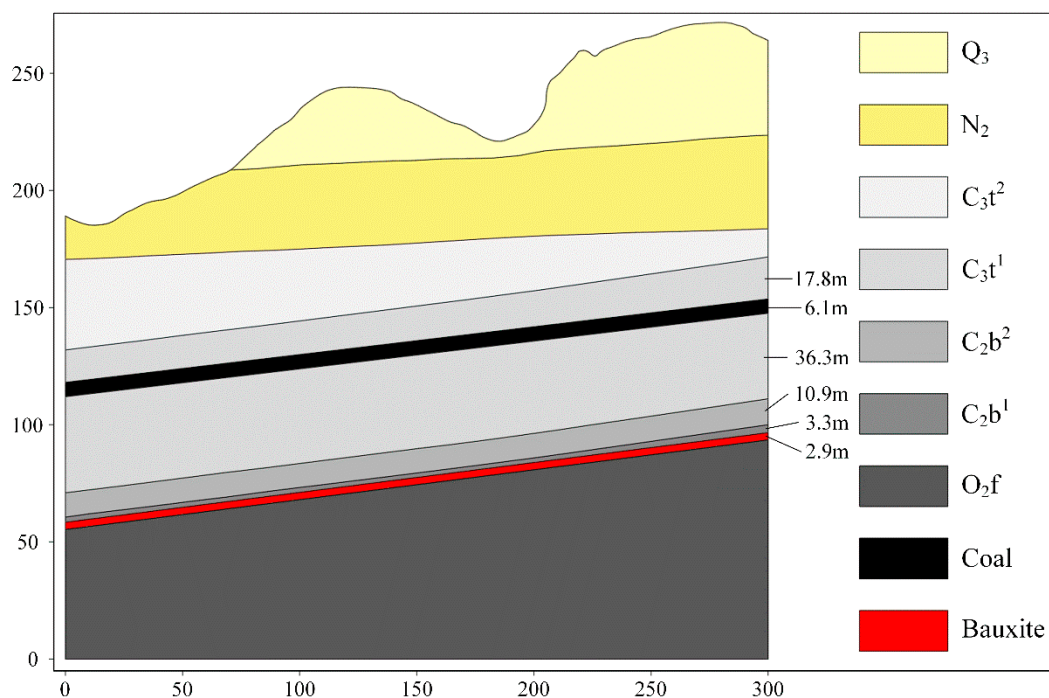


Figure 4. Engineering geological condition of BCS.

The rock mechanic parameters used in the numerical simulation are from the verification report of resources and reserves, while the mechanical parameters of two-step RCB are obtained from the mixture proportion tests and laboratory mechanical tests (see Figure 2a). For RCB, S95 slag powder (account for 90%) is used as the cementitious material and lime (account for 10%) as the activator. In the first and second step, the cement–sand ratio of RCB is 1:6 and 1:12, respectively, and the mass concentration is 60%. The mechanical parameters of each material are shown in Table 3. Among them, the results of RCB were measured after 28 days of curing.

Table 3. Mechanical parameters of rocks and backfilling body.

Rock Layer Code	Elastic Modulus (GPa)	Compressive Strength (MPa)	Tensile Strength (MPa)	Poisson Ratio	Bulk Density ($\text{kN}\cdot\text{m}^{-3}$)	Cohesion (MPa)	Internal Friction Angle ($^{\circ}$)
Q ₃	0.33	1.18	0.21	0.33	17.46	0.13	21.60
N ₂	0.38	2.07	0.24	0.31	17.85	0.19	22.35
C _{3t} ²	73.81	35.70	0.84	0.28	25.41	3.12	44.00
C _{3t} ¹	75.40	46.40	1.00	0.30	26.19	3.66	42.63
Coal seam	0.99	4.74	0.50	0.29	13.73	1.05	28.10
C _{2b} ²	20.48	11.80	0.72	0.32	24.92	1.29	27.65
C _{2b} ¹	18.34	61.30	0.48	0.33	23.15	0.97	28.35
Bauxite	69.32	131.30	2.70	0.28	26.68	18.53	41.15
O _{2f}	77.40	146.00	1.85	0.36	26.39	5.54	48.70
First step RCB	0.91	2.52	0.48	0.26	19.23	0.34	49.85
Second step RCB	0.53	1.74	0.27	0.31	18.93	0.22	42.62

3.2. Model Construction and Variable Selection

Due to the lack of surface data in the study area, in order to simulate the mining process of a complete panel, the two-dimensional section of Figure 4 was stretched to establish a three-dimensional model, and the grid was reasonably divided and imported to the FLAC^{3D} software. The final numerical analysis model of BCS is shown in Figure 5, and the bottom dimension of the model is 300 m × 300 m, and the highest roof is 272 m above the bottom. All of the overlying strata are included in the model, the bauxite layer

is divided into three mining areas, and the middle of the mining area is separated by 10 m-wide pillars. According to the two-step interval process of IDBM, the mining strips are arranged perpendicular to the orebody strike and divided into two steps, with a stope width of 4 m, height of 3 m, and length of 50 m. The model boundary is large enough that the impact of the model boundary could be ignored. Therefore, we used the FIX command to limit the displacement of the bottom and side surfaces of the model to zero. In FLAC^{3D} software for numerical analysis, the elastic–plastic material model was chosen, and the Mohr–Coulomb yield criterion was selected to judge material failure [29]. The shear failure surface is simplified as a linear failure surface, which can be expressed by Equations (1) and (2):

$$f_s = \sigma_1 - \sigma_3 N_\varphi + 2c\sqrt{N_\varphi} \quad (1)$$

$$f_t = \sigma_3 - \sigma_1 \quad (2)$$

where σ_1 is the maximum principal stress; σ_3 is the minimum principal stress; c is cohesion; φ is internal friction angle; $N_\varphi = (1 + \sin\varphi)/(1 - \sin\varphi)$. Additionally, when $f_s = 0$, shear failure occurs; when $f_t = 0$, tensile failure occurs.

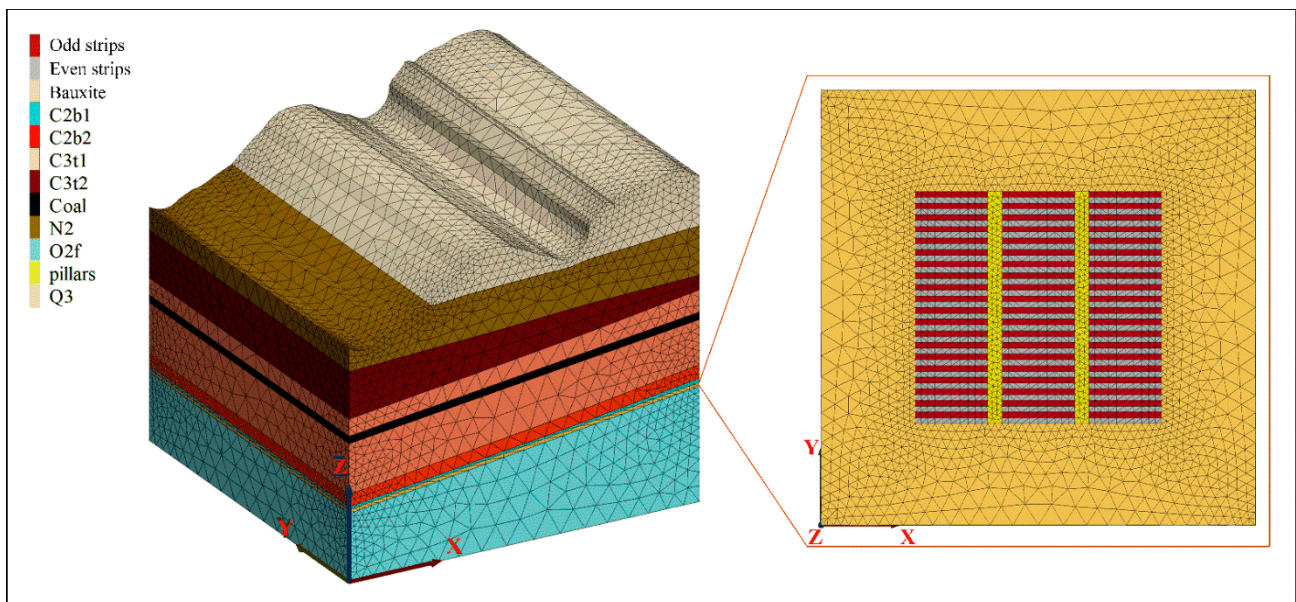


Figure 5. Numerical analysis model of BCS.

3.3. Simulation Plan and Process

As the first step of the FLAC^{3D} simulation, the initial equilibrium state with a maximum unbalanced force of less than 1.0×10^{-5} N is calculated based on the gravity field condition under the maximum premise value of material parameters. Then, the displacement velocity element state is returned to zero, so as to obtain the initial stress condition [30]. Under the premise of not mining coal seam and only mining bauxite for the time being, the main steps of FLAC^{3D} simulation are carried out according to the following three mining conditions:

- (1) Simulation of the non-mining condition. According to the given material parameters of each rock layer, the final equilibrium state of the model with a maximum unbalanced force of less than 1.0×10^{-5} N is calculated directly.
- (2) Simulation of the normal backfilling condition according to the two-step interval process of IDBM. First, the odd mining strips are mined out and calculated for ten steps based on the given material parameters of each rock layer. Second, the odd mining strips are backfilled with the first step RCB and calculated for ten steps. Further, the even mining strips are mined out and calculated for ten steps. Finally,

the even mining strips are backfilled with the second step RCB and calculated for the final equilibrium state.

- (3) Simulation of the non-backfilling condition to the equilibrium state. The most dangerous mining condition happens when the even mining strips are mined out while the second step RCB is cancelled.

4. Numerical Simulation Results and Analysis

According to the above simulation plan and process, the numerical simulation results are obtained and used for analyzing the feasibility of RCB for the safe mining of BCS.

4.1. Distribution of Principal Stress

Cutting from the middle of the model along the direction of the mining strips, the distributions of maximum principal stress and minimum principal stress are obtained and shown in Figures 6 and 7, respectively.

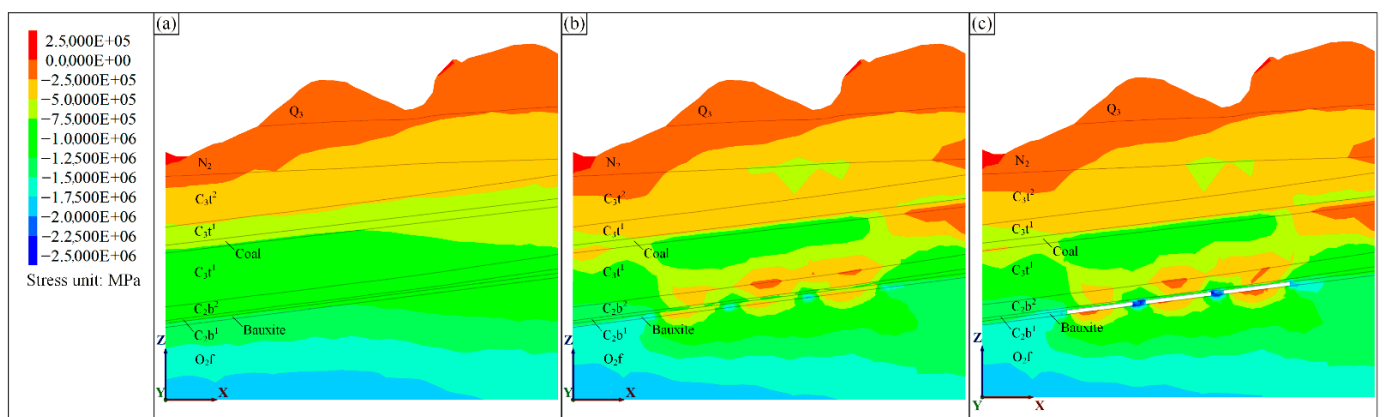


Figure 6. Distribution of maximum principal stress: (a) non-mining condition; (b) normal backfilling condition; (c) non-backfilling condition.

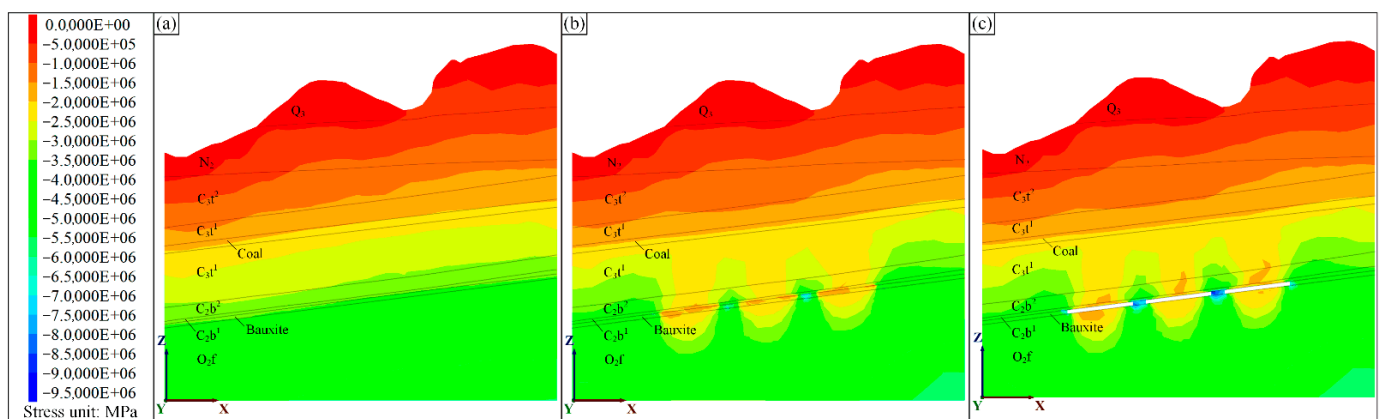


Figure 7. Distribution of minimum principal stress: (a) non-mining condition; (b) normal backfilling condition; (c) non-backfilling condition.

As we can see from Figures 6a and 7a, the distributions of maximum principal stress and minimum principal stress under the non-mining condition are originally distributed like layers and decreased from top to bottom. As for the normal backfilling condition, the principal stress was redistributed after mining disturbance and backfill (see Figures 6b and 7b), and there are obvious differences between the stress conditions of the pillar and RCB. The maximum principal stress and minimum principal stress of the pillar are significantly lower than that of RCB, and both of them are negative, which indicates

that the pillar is mainly subject to the compression action. Under the non-backfilling condition (see Figures 6c and 7c), the maximum principal stress in the middle of the roof and floor decreases, while the maximum principal stress of pillar improves significantly, which is called the local tensile stress concentration. Since the maximum principal stress is changed from negative to positive during this condition, the pillar is more prone to plastic deformation and collapse failure, endangering mining safety. Therefore, the backfilling treatment of mining strips can greatly alleviate the compression state of pillars and avoid serious tensile stress concentration of the roof and floor.

4.2. Distribution of Displacement and Plastic Zone

Cutting at the same position, the distribution of Z-direction displacement under the non-mining condition (see Figure 8a), the normal backfilling condition (see Figure 8b), and the non-backfilling condition (see Figure 8c) are obtained, respectively. Compared with Figure 8a,b, backfill mining will cause little floor displacement and obvious roof displacement, especially in the middle of the roof, which is a consequence of the local tensile stress concentration. Compared with the non-backfilling condition, the maximum roof displacement of normal backfill mining is only 50% of that of non-backfilling, while the roof displacement range is only 30% of that of non-backfilling.

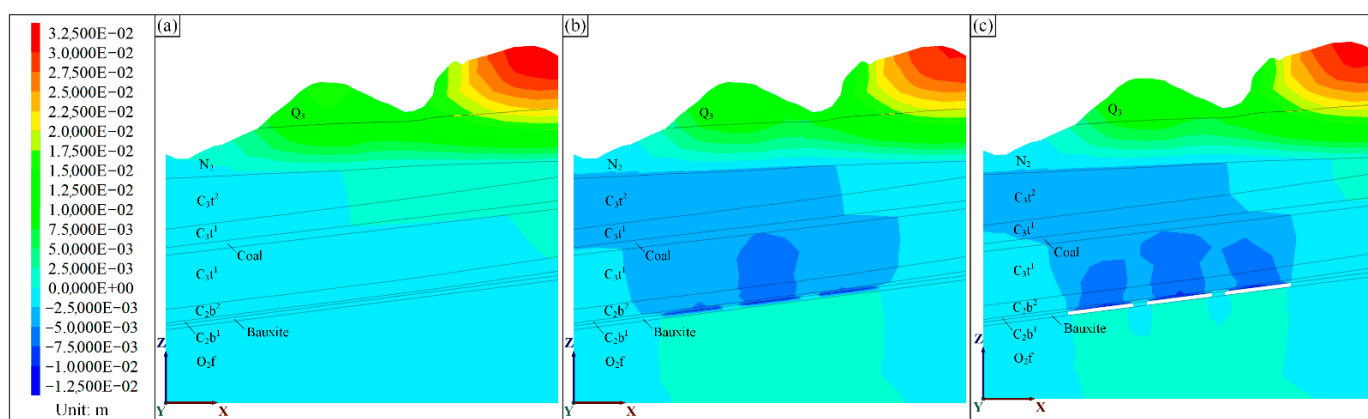


Figure 8. Distribution of Z-direction displacement: (a) non-mining condition; (b) normal backfilling condition; (c) non-backfilling condition.

Since the average ultimate tensile strength of the ore direct roof C_{2b}^1 is very low, the roof will be exposed and easily tensile-damaged once the bauxite is mined out. Extensive crack propagation may cut through the overlying coal seam and cause gas outburst disaster, endangering mining safety. Therefore, more attention should be paid to the ore direct roof C_{2b}^1 during this numerical simulation. By hiding the other strata, except for the C_{2b}^1 stratum, the distribution of the plastic zone along the Z-direction under the non-mining condition (see Figure 9a), normal backfilling condition (see Figure 9b), and non-backfilling condition (see Figure 9c) are obtained, respectively.

As we can see from Figure 9, no roof unit is damaged under the non-mining condition, while a certain amount of partial failure units will occur in the roof under the normal backfilling condition. Most of the partial failure units belong to tensile failure and are caused by the local tensile stress concentration, which is consistent with previous analysis. Since the number of failure units is limited and has not formed a penetrating area, the roof damage can be contained easily during the normal backfilling process. In contrast, there are a great many tensile-damaged units in the case of the non-backfilling condition, and several penetrating areas have formed and just corresponded to the position of mining strips.

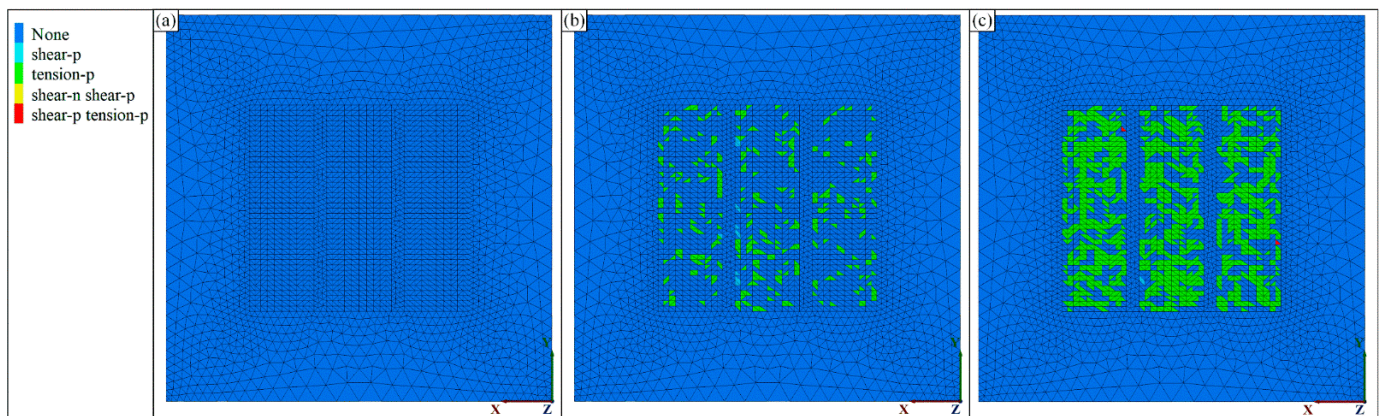


Figure 9. Distribution of plastic zone: (a) non-mining condition; (b) normal backfilling condition; (c) non-backfilling condition.

4.3. Extreme Values of Principal Stress and Displacement

The extreme values of the maximum principal stress of the roof and the minimum principal stress of the pillar can be obtained from Figures 8 and 9. The maximum displacement of the roof in Z-direction can be obtained from Figure 7. Under non-mining, normal backfilling, and non-backfilling conditions, the extreme values of bauxite and coal are listed in Table 4. Meanwhile, the line charts of these extreme values are drawn and shown in Figure 10.

Table 4. Extreme values of principal stress and displacement under different mining conditions.

Model Location	Condition	Maximum Principal Stress of Roof (MPa)	Minimum Principal Stress of Pillar (MPa)	Maximum Displacement of Roof in Z-Direction (cm)
Bauxite	Non-mining	−0.9228	−1.1236	−0.0283
	Normal backfilling	−0.1992	−6.9180	−0.9009
	Non-backfilling	0.4956	−9.3295	−1.2322
Coal seam	Non-mining	−0.4863	−2.1303	−0.0068
	Normal backfilling	−0.3942	−1.9428	−0.3416
	Non-backfilling	−0.4139	−1.9480	−0.4965

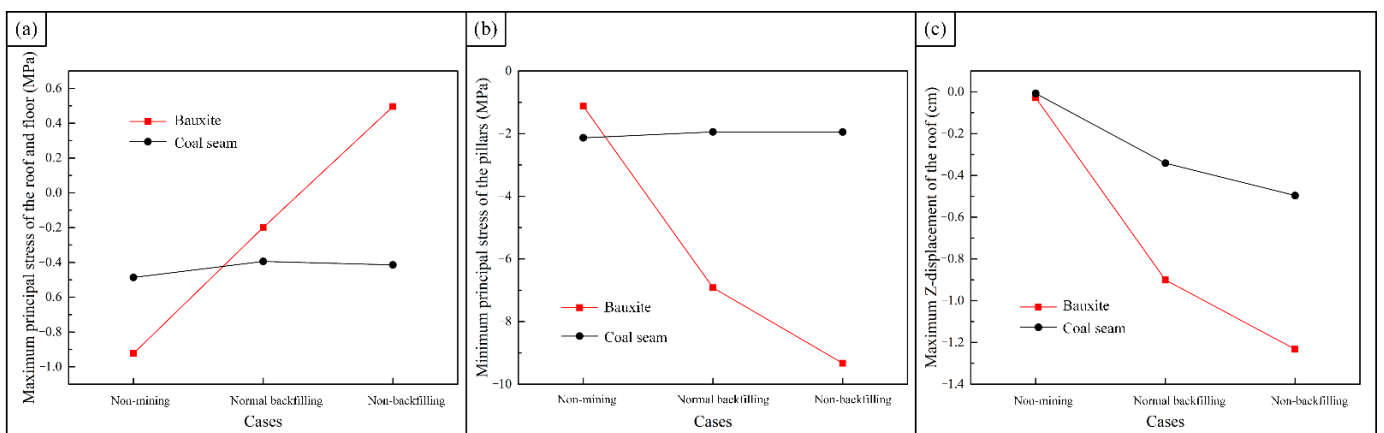


Figure 10. Charts of extreme values: (a) maximum principal stress of roof; (b) minimum principal stress of pillar; (c) maximum displacement of roof in Z-direction.

It can be seen from Table 4 that the mining disturbance redistributes the in-situ stress field of overlying strata and changes the bauxite roof and floor stress state from compression to tension and the pillar stress state from common compression to the local tensile stress concentration. Normal backfilling can not only reduce the pressure stress of pillars, but also release the tensile stress in the roof and floor from positive to negative, effectively preventing roof subsidence. For example, the maximum principal stress of a bauxite roof under normal backfilling conditions is -0.1992 MPa, while that of non-backfilling conditions is $+0.4956$ MPa. The minimum principal stress of a bauxite pillar under normal backfilling conditions is -6.9180 MPa, which is reduced by 26% than that of non-backfilling conditions.

It can be seen from Figure 10 that backfilling mining has an obvious influence on the maximum displacement of the roof in Z-direction. For example, the maximum displacement of the bauxite roof in Z-direction under the normal backfilling condition is -0.9009 cm, while that of the non-backfilling is -1.2322 cm. The maximum displacement of a coal seam roof in Z-direction under the normal backfilling condition is -0.3416 cm, which is reduced by 31% of that of the non-backfilling condition. As long as the mining strips are backfilled in time after being mined out, the roof tensile failure can be prevented from developing effectively, and the serious tensile stress concentration of pillars will be avoided. Therefore, RCB shows excellent superiority in ground pressure management and mining safety guarantees, and the RCB mining technology of layered soft BCS is technically feasible and economically reasonable.

5. Coupling Mechanism Analysis of Paste Backfill and Layered Soft Rocks

Layered rock mass with different failure forms exists widely in steep slope and underground mining engineering [31]. Microscopically, the failure of the layered rock mass can be divided into five forms, including penetrating shear failure, bedding shear failure, composite shear failure, bedding sliding failure, and compression distortion failure [32]. The overlying strata of bauxite, which belong to typical plate-cracking structural rocks, are refractory clay ore, sandy clay rock, coal seam, thin layer sandstone, black mudstone, and other soft, brittle rocks. Its particularity is that even if the stress is not too high, structural failure and instability may occur [33]. The layered soft rocks tend to exhibit structural rather than material destruction, which is manifested in the phenomenon of roof bending, side collapse, floor heave, and so on [34].

As shown in Figure 11a, if bauxite ore is mined by the traditional open-stope method, then a large number of pillars will be left in a stope to support the roof [35]. Since the stability of pillars deteriorates sharply under the continuous action of blasting vibration, weathering, and leaching, these high-quality resources will be difficult to recover with the passage of time, resulting in permanent losses [36]. Meanwhile, continuous high-strength mining of bauxite will also produce large-scale goafs, easily causing roof fall and side collapse accidents. As a result, these accidents may lead to caving zones, fissure zones, and bending subsidence zones occurring in the above clay layer [37], as shown in Figure 11b. Extensive crack propagation may cut through the overlying coal seam and cause gas outburst disaster, endangering mining safety. In addition, large-scale goafs may also lead to surface subsidence and collapse, causing serious damage to surface rivers, highways, and structures [38].

As shown in Figure 11c, backfilling has been recognized as an excellent method for goaf disposal and ground pressure management [39]. Paste backfill entering goafs interacts with surrounding rocks after osmotic dehydration and consolidation hardening, then a series of complex interactions will make a difference [40]. First, crack propagation and large deformation can be effectively suppressed by paste backfill for sealing the releasing face of elastic potential energy. Secondly, broken soft rocks can be supported by paste backfill to provide lateral pressure on the slip trend. Additionally, under the action of interfacial frictions between paste backfill and side rocks, partial self-weight stress of roofs can be transferred and the closure trend of stopes will be suppressed [41].

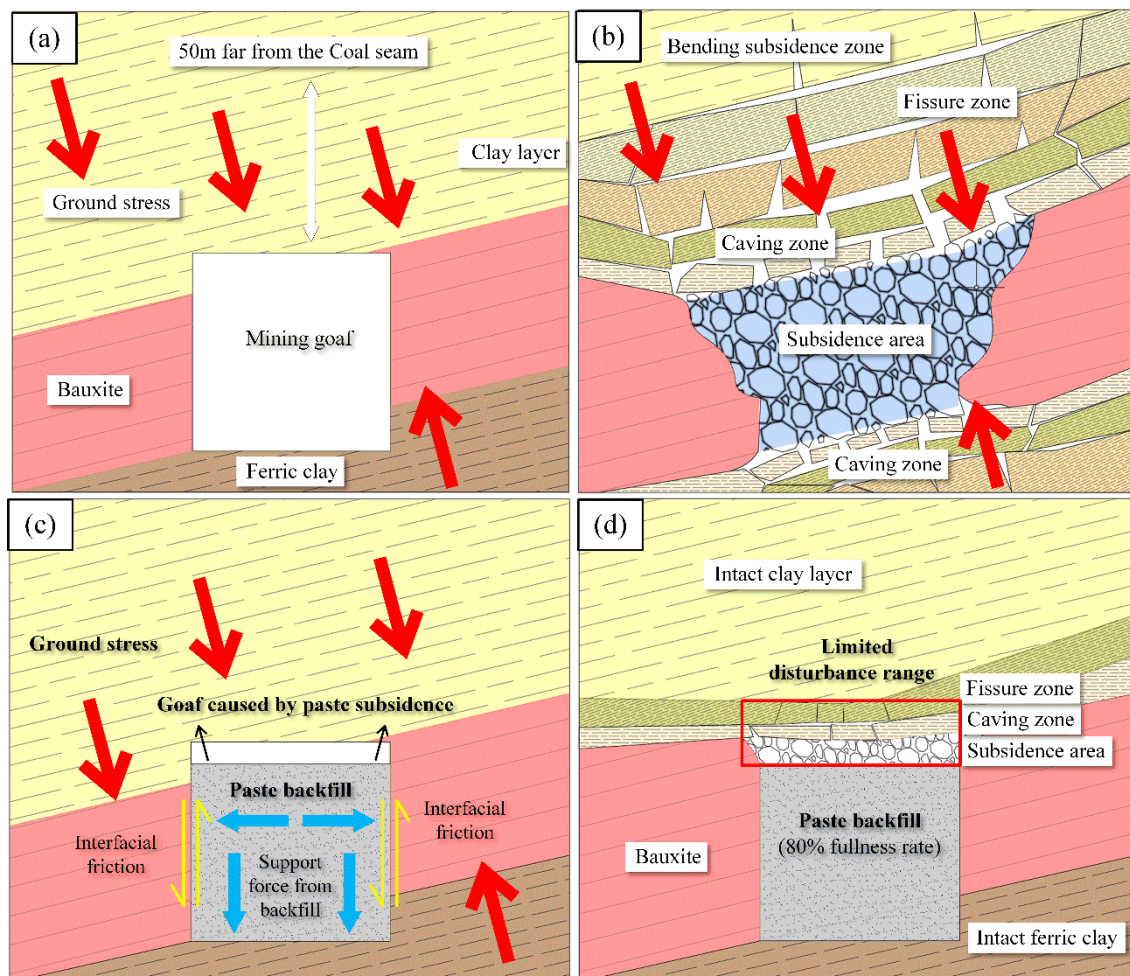


Figure 11. Failure process of layered soft rocks and mechanism analysis of paste backfill: (a) goaf after mining; (b) collapsed goaf; (c) goaf after paste backfill (d) stable goaf.

Subject to the uneven stope roof and paste backfill sinking, there will be an unconnected area of 0.1–0.3 m above the backfill body (see Figure 11d), but paste backfill can still play an excellent supporting role and effectively control the roof disturbance within 3 m. Although limited unconnected areas may cause the structural failure of direct roofs, a certain extent of roof failure is beneficial to alleviate the stress concentration and block the disaster chain effect of rock burst, which is known to be caused by the accumulation and sudden violent release of the surrounding strain energy [42]. Meanwhile, due to the crushing expansion character of rocks [43], a small amount of roof collapse rocks can fill the unconnected 0.1–0.3 m area, thus completely eliminating the hidden danger of goafs and closing the release surface of strain energy. In addition, the combined bearing structure of collapsed rocks and backfill body is both rigid and flexible, which has the advantages of high stiffness from rigid rocks, and a large buffering effect from the backfill body. Since creep damage of the flexible backfill body will absorb and dissipate lots of energy, the overall effect of collapsed rock and the backfill body is better than that of single rigid rocks [44].

6. Conclusions

This study explored the feasibility of recycling BRM as a backfilling aggregate for the safe and efficient mining of layered soft BCS. A series of tests were conducted to prevent the pollution diversion of BRM from surface storage to underground goafs, and avoid polluting the groundwater. A numerical simulation analysis of the backfilling mining

process was carried out based on the FLAC^{3D} software to protect the overlying coal seam and ensure mining safety. The following conclusions were drawn.

- (1) As a strong alkaline solid waste produced by alumina industry, BRM contains plenty of alumina, iron oxide, titanium dioxide, sodium oxide, and calcium oxide, which are difficult to remove and easy to pollute the surface environment by open storage. Since PO 42.5 cement shows a slow solidifying rate and low early strength when mixed with BRM, S95 slag powder and lime were evenly mixed with BRM with a cement–sand ratio of 1:6 and 60% mass concentration, which solidified quickly within 12 h and reached a high strength of 1.1 MPa in 7 days.
- (2) Under the action of encapsulation, solidification, and inhibiting precipitation from cementitious materials, the bleeding rate of RCB is only 5% and the leaching concentration of harmful substances can be reduced by 70% more than fresh BRM. After flowing into a water sump through a gutterway, the bleeding water can be further diluted at least 50–100 times to the Grade I groundwater standard of China, and finally discharged to a surface sewage tank for centralized purification and recycling. Therefore, RCB is technically feasible, economical, and reasonable, and has significant environmental protection and safety demonstration effects.
- (3) Taking a typical bauxite mine in Shanxi as an example, a three-dimensional model was constructed by FLAC^{3D} software, the IDBM was selected as the main mining method, and the Mohr–Coulomb yield criterion was selected to judge material failure. The results show that backfill mining will cause little floor displacement and limited roof displacement; the maximum roof displacement of normal backfill mining is only 50% of that of non-backfilling, while the roof displacement range is only 30% of that of non-backfilling.
- (4) Mining disturbance redistributes the in-situ stress field of overlying strata; normal backfilling can not only reduce the pressure stress of pillars, but also release the tensile stress in the roof and floor from positive to negative, effectively preventing roof subsidence. The maximum principal stress of bauxite roof under normal backfilling conditions is -0.1992 MPa, while that of non-backfilling is $+0.4956$ MPa. The maximum displacement of a coal seam roof in Z-direction under normal backfilling conditions is -0.3416 cm, which is reduced by 31% more than that of non-backfilling condition.
- (5) Layered soft BCS belongs to typical plate-cracking structural rocks, the structural failure and instability of which may occur even if the stress is not too high. Continuous high-strength mining of bauxite will produce large-scale goafs, easily causing roof fall and side collapse accidents, and may also cut through the overlying coal seam and cause gas outburst disaster. Since creep damage processes will absorb and dissipate lots of energy, past backfill shows excellent superiority in goaf disposal and ground pressure management. Under the overall effect of collapsed rock and the backfill body, the disturbance range of IDBM is controlled within 3 m, which is only 10% of the open-stope method.

Author Contributions: Conceptualization, S.L. and B.H.; data curation, R.Z., R.F., G.W. and H.Y.; formal analysis, R.Z., R.F., G.W. and H.Y.; methodology, S.L. and B.H.; project administration, S.L.; software, S.L. and B.H.; validation, S.L.; visualization, B.H.; writing—original draft, S.L., R.Z. and B.H.; writing—review and editing, S.L. and B.H. All authors have read and agreed to the published version of the manuscript.

Funding: This research was funded by the National Natural Science Foundation of China (51804337).

Institutional Review Board Statement: Not applicable.

Informed Consent Statement: Not applicable.

Data Availability Statement: The data presented in this study are available on request from the corresponding author.

Conflicts of Interest: The authors declare no conflict of interest.

References

1. Machado, J.A.R. *Advanced Hydraulic Characterization of Treated and Untreated Bauxite Residue Study Using Steady State Centrifugation*; California State University: Los Angeles, CA, USA, 2020.
2. Kalaitzidis, S.; Siavalas, G.; Skarpelis, N.; Araujo, C.V.; Christanis, K. Late Cretaceous coal overlying karstic bauxite deposits in the Parnassus-Ghiona Unit, Central Greece: Coal characteristics and depositional environment. *Int. J. Coal Geol.* **2010**, *81*, 211–226. [[CrossRef](#)]
3. Cui, Y.; Chen, J.; Zhang, Y.; Peng, D.; Huang, T.; Sun, C. pH-dependent leaching characteristics of major and toxic elements from red mud. *Int. J. Environ. Res. Public Health* **2019**, *16*, 2046. [[CrossRef](#)]
4. Huang, W.; Wang, S.; Zhu, Z.; Li, L.; Yao, X.; Rudolph, V.; Haghseresht, F. Phosphate removal from wastewater using red mud. *J. Hazard. Mater.* **2008**, *158*, 35–42. [[CrossRef](#)]
5. Cheng, X.; Long, D.; Zhang, C.; Gao, X.; Yu, Y.; Mei, K.; Zhang, C.; Guo, X.; Chen, Z. Utilization of red mud, slag and waste drilling fluid for the synthesis of slag-red mud cementitious material. *J. Clean. Prod.* **2019**, *238*, 117902. [[CrossRef](#)]
6. Doodoo-Arhin, D.; Konadu, D.S.; Annan, E.; Buabeng, F.P.; Yaya, A.; Agyei-Tuffour, B. Fabrication and characterisation of Ghanaian bauxite red mud-clay composite bricks for construction applications. *Am. J. Mater. Sci.* **2013**, *3*, 110–119.
7. Xu, X.; Song, J.; Li, Y.; Wu, J.; Liu, X.; Zhang, C. The microstructure and properties of ceramic tiles from solid wastes of Bayer red muds. *Constr. Build. Mater.* **2019**, *212*, 266–274. [[CrossRef](#)]
8. Mukiza, E.; Zhang, L.L.; Liu, X.; Zhang, N. Utilization of red mud in road base and subgrade materials: A review. *Resour. Conserv. Recycl.* **2019**, *141*, 187–199. [[CrossRef](#)]
9. Chen, X.; Guo, Y.; Ding, S.; Zhang, H.Y.; Xi, F.Y.; Wang, J.; Zhou, M. Utilization of red mud in geopolymer-based pervious concrete with function of adsorption of heavy metal ions. *J. Clean. Prod.* **2019**, *207*, 789–800. [[CrossRef](#)]
10. Ozden, B.; Brennan, C.; Landsberger, S. Investigation of bauxite residue (red mud) in terms of its environmental risk. *J. Radioanal. Nucl. Chem.* **2019**, *319*, 339–346. [[CrossRef](#)]
11. Nie, Q.; Hu, W.; Huang, B.; Shu, X.; He, Q. Synergistic utilization of red mud for flue-gas desulfurization and fly ash-based geopolymer preparation. *J. Hazard. Mater.* **2019**, *369*, 503–511. [[CrossRef](#)] [[PubMed](#)]
12. Ghirian, A.; Fall, M. Coupled behavior of cemented paste backfill at early ages. *Geotech. Geol. Eng.* **2015**, *33*, 1141–1166. [[CrossRef](#)]
13. Pokharel, M.; Fall, M. Combined influence of sulphate and temperature on the saturated hydraulic conductivity of hardened cemented paste backfill. *Cem. Concr. Compos.* **2013**, *38*, 21–28. [[CrossRef](#)]
14. Sun, W.; Wu, A.; Wang, H.; Li, T.; Liu, S. Experimental study on the influences of sodium sulphide on zinc tailings cement paste backfill in Huize Lead-Zinc Mine. *Int. J. Min. Miner. Eng.* **2015**, *6*, 119–138. [[CrossRef](#)]
15. Yin, Y.; Zhao, T.; Zhang, Y.; Tan, Y.; Qiu, Y.; Taheri, A.; Jing, Y. An innovative method for placement of gangue backfilling material in steep underground coal mines. *Minerals* **2019**, *9*, 107. [[CrossRef](#)]
16. Sheshpari, M. A review of underground mine backfilling methods with emphasis on cemented paste backfill. *Electron. J. Geotech. Eng.* **2015**, *20*, 5183–5208.
17. Wang, X.; Zhao, B.; Zhang, Q. Cemented backfill technology based on phosphorous gypsum. *J. Cent. South Univ. Technol.* **2009**, *16*, 285–291. [[CrossRef](#)]
18. Jiang, H.; Fall, M.; Yilmaz, E.; Li, Y.; Yang, L. Effect of mineral admixtures on flow properties of fresh cemented paste backfill: Assessment of time dependency and thixotropy. *Powder Technol.* **2020**, *372*, 258–266. [[CrossRef](#)]
19. Razak, H.A.; Naganathan, S.; Hamid, S.N.A. Controlled low-strength material using industrial waste incineration bottom ash and refined kaolin. *Arab. J. Sci. Eng.* **2010**, *35*, 53–67.
20. Vigneshwaran, S.; Uthayakumar, M.; Arumugaprabu, V. Potential use of industrial waste-red mud in developing hybrid composites: A waste management approach. *J. Clean. Prod.* **2020**, *276*, 124278. [[CrossRef](#)]
21. Jewell, R.; Fourie, A. *Paste and Tickened Tailings—A Guide*, 3rd ed; Australian Centre for Geomechanics: Perth, Australia, 2015.
22. Khairul, M.A.; Zanganeh, J.; Moghtaderi, B. The composition, recycling and utilisation of Bayer red mud. *Resour. Conserv. Recycl.* **2019**, *141*, 483–498. [[CrossRef](#)]
23. Sofrá, F.; Boger, D.V. Environmental rheology for waste minimisation in the minerals industry. *Chem. Eng. J.* **2002**, *86*, 319–330. [[CrossRef](#)]
24. Sutar, H.; Mishra, S.C.; Sahoo, S.K.; Chakraverty, A.P.; Maharana, S.H. Progress of red mud utilization: An overview. *Am. Chem. Sci. J.* **2014**, *4*, 255–279. [[CrossRef](#)]
25. Cihangir, F.; Ercikdi, B.; Kesimal, A.; Ocak, S.; Akyol, Y. Effect of sodium-silicate activated slag at different silicate modulus on the strength and microstructural properties of full and coarse sulphidic tailings paste backfill. *Constr. Build. Mater.* **2018**, *185*, 555–566. [[CrossRef](#)]
26. Wang, L.; Chen, L.; Tsang, D.C.W.; Zhou, Y.; Rinklebe, J.; Song, H.; Kwon, E.E.; Baek, K.; Ok, Y.S. Mechanistic insights into red mud, blast furnace slag, or metakaolin-assisted stabilization/solidification of arsenic-contaminated sediment. *Environ. Int.* **2019**, *133*, 105247. [[CrossRef](#)]
27. Gao, L.; Li, J.; Wang, D.; Xiong, X.; Yi, C.; Han, M. Outline of metallogenic regularity of bauxite deposits in China. *Acta Geol. Sin.* **2015**, *89*, 2072–2084.
28. Bin, Z. Evaluation Geologic Features and Resource Potential of Gaojian Mountain Mining Area Bauxite in Qinyuan County. *Sci. Technol. Innov. Product.* **2013**, *2*, 105–107.

29. Gedela, R.; Karpurapu, R. Influence of Pocket Shape on Numerical Response of Geocell Reinforced Foundation Systems. *Geosynth. Int.* **2020**, *28*, 327–337. [[CrossRef](#)]
30. Dong, L. Application of Upward In-strips Drift Cut-fill Method in Wangershan Gold Mine. *Met. Mine.* **2005**, *1*, 26–28.
31. Taliercio, A.; Landriani, G.S. A failure condition for layered rock. *Int. J. Rock Mech. Min. Sci. Geomech. Abstr. Pergamon* **1988**, *25*, 299–305. [[CrossRef](#)]
32. Zhao, J.; Zhang, Y. Studies on rock failure of layered rock in underground mining-face and control techniques. *Geomech. Geophys. Geo-Energy Geo-Resour.* **2017**, *3*, 405–414. [[CrossRef](#)]
33. Sher, E.N. Determination of shapes and sizes of radial cracks formed by blasthole charges and hydraulic fracturing in a layered rock mass. *IOP Conf. Ser. Earth Environ. Sci.* **2021**, *773*, 012025. [[CrossRef](#)]
34. Zhao, C.X.; Li, Y.M.; Liu, G.; Meng, X. Mechanism analysis and control technology of surrounding rock failure in deep soft rock roadway. *Eng. Fail. Anal.* **2020**, *115*, 104611. [[CrossRef](#)]
35. Sipeki, L.; Newman, A.M.; Yano, C.A. Selecting support pillars in underground mines with ore veins. *IISE Trans.* **2020**, *52*, 1173–1188. [[CrossRef](#)]
36. Xiao, C.; Zheng, H.; Hou, X.; Zhang, X. A stability study of goaf based on mechanical properties degradation of rock caused by rheological and disturbing loads. *Int. J. Min. Sci. Technol.* **2015**, *25*, 741–747. [[CrossRef](#)]
37. Jiang, L.; Yang, C.; Jiao, H. Ultimately exposed roof area prediction of bauxite deposit goaf based on macro joint damage. *Int. J. Min. Sci. Technol.* **2020**, *30*, 699–704. [[CrossRef](#)]
38. Deng, J.; Bian, L. Investigation and characterization of mining subsidence in Kaiyang Phosphorus Mine. *J. Cent. South Univ. Technol.* **2007**, *14*, 413–417. [[CrossRef](#)]
39. Feng, X.; Zhang, Q. The effect of backfilling materials on the deformation of coal and rock strata containing multiple goaf: A numerical study. *Minerals* **2018**, *8*, 224. [[CrossRef](#)]
40. Yilmaz, E.; Belem, T.; Bussi ere, B.; Mbonimpa, M.; Benzaazoua, M. Curing time effect on consolidation behaviour of cemented paste backfill containing different cement types and contents. *Constr. Build. Mater.* **2015**, *75*, 99–111. [[CrossRef](#)]
41. le Roux, K.; Bawden, W.F.; Grabinsky, M.F. Field properties of cemented paste backfill at the Golden Giant mine. *Min. Technol.* **2005**, *114*, 65–80. [[CrossRef](#)]
42. Wang, G.-F.; Gong, S.-Y.; Li, Z.-L.; Dou, L.M.; Cai, W.; Mao, Y. Evolution of stress concentration and energy release before rock bursts: Two case studies from Xingan coal mine, Hegang, China. *Rock Mech. Rock Eng.* **2016**, *49*, 3393–3401. [[CrossRef](#)]
43. Rebeka, M.I. The interrelation of petrographical properties of rocks and their crushing and grinding features: A literature review. *Multidiszcip. Tudom nyok* **2021**, *11*, 17–24.
44. Gong, P.; Ma, Z.; Ni, X.; Zhang, R.R. Floor heave mechanism of gob-side entry retaining with fully-mechanized backfilling mining. *Energies* **2017**, *10*, 2085. [[CrossRef](#)]